Investigation of 1064-nm Pumped Type II SPDC in Potassium Niobate for Generation of High Spectral Purity Photon Pairs

Donghwa Lee, Ilhwan Kim and Kwang Jo Lee *

Department of Applied Physics, Institute of Natural Science, Kyung Hee University, Yongin-si 17104, Korea; fairytale095@gmail.com (D.L.); dlfghks383@gmail.com (I.K.)
* Correspondence: kjlee88@khu.ac.kr

Abstract: The generation and detection of nonclassical light of about 2 μm has good potential in an emerging field of high-sensitivity metrology, especially gravitational wave detection, as well as free-space quantum communication. A pair of photons is generated through a spontaneous parametric down-conversion (SPDC) process in a nonlinear optic crystal, which can be properly entangled in a spatial region where two beams with each polarization overlap or in a Sagnac-loop interferometer configuration. We investigated theoretically and numerically Type II SPDC in a potassium niobate ($KNbO_3$, KN) crystal, which is useful as a material platform for generating photon pairs of high spectral purity in the 2-μm range. The technique is based on the frequency degenerate SPDC under Type II extended phase matching (EPM). We described the EPM characteristics of KN and showed that it is practically feasible for a 1064-nm pumped SPDC under moderate temperature conditions. The effective nonlinear optic coefficient of KN is at least four-times larger than those of other crystals using the Type II EPM approach, which implies a significant improvement in SPDC efficiency. The joint spectral analysis showed that a pair of photons can be generated with a high purity of 0.995 through proper pump filtering.

1. Introduction

The generation and detection of nonclassical light of about 2 μm has good potential in an emerging field of high-sensitivity metrology, especially in gravitational wave detection [1–3]. Such long wavelengths can reduce quantum noise and scattering losses in interferometric gravitational wave detectors such as the laser interferometer gravitational wave observatory (LIGO)-Voyager [4]. Since this 2-μm band belongs to a window of high transparency in the atmospheric absorption spectrum, quantum light sources in this band also have great potential for applications such as free space quantum communication and sensing, with the advantages of high sensitivity and low noise measurement [4–6]. Mansell et al. utilized a combination of a second-harmonic generator and an optical parametric oscillator with two pieces of periodically poled potassium titanyl phosphates (PPKTPs) to generate nonclassical squeezed states of light [1]. Prabhakar et al. demonstrated two-photon quantum interference and entanglement at 2.1 μm using Type 0 spontaneous parametric down-conversion (SPDC) in a magnesium oxide-doped periodically poled lithium niobate (MgO:PPLN) [3]. In future studies, the basic requirements of the platform for generating photon pairs in the 2-μm spectral range can be listed as follows: (1) SPDC using the frequency-degenerate Type II extended phase matching (EPM) is desirable for the generation of high spectral purity photon pairs. Here, the EPM refers to the simultaneous achievement of phase matching (PM) and group velocity (GV) matching between interacting photons [7,8]. In addition, two photons generated simultaneously via Type II SPDC have polarization states that are perpendicular to each other. In this case, the

polarization-entanglement can be obtained in the spatial region where two beams (or cones) with each polarization overlap, or in a Sagnac-loop interferometer configuration [9–11]. (2) A prevalent commercial laser is preferred as a light source for SPDC pumping to generate photon pairs in the 2-μm band. Coherent light sources with a wavelength of about 1 μm that are suitable for SPDC pumping include distributed feedback lasers, Fabry-Pérot lasers, and Yb-doped fiber lasers, but the most widely used high power and stable lasers are solid-state Nd:YAG (neodymium-doped yttrium aluminum garnet, $Nd:Y_3Al_5O_{12}$) lasers. For example, 1064-nm Nd:YAG lasers are used in a variety of applications in science and technology, especially in materials processing, medicine, spectroscopy, and other laser pumping [12]. The wavelength of the photon pairs generated via the SPDC pumped by the Nd:YAG laser is 2128 nm, which is within the high transparency range in the atmospheric absorption spectrum [5]. (3) The larger the nonlinearity of the crystal used for SPDC, the higher the SPDC efficiency. The SPDC efficiency is proportional to the square of the effective nonlinear optic coefficient for the given EPM condition [13]. However, the 1064-nm pumped SPDC of the Type II EPM approach has not yet been reported to the best of our knowledge. Now, it is timely to find suitable candidates for nonlinear optic crystals that satisfy all of the requirements listed above and investigate their usefulness as a generator of photon pairs in the 2-μm band. In this paper, we theoretically and numerically investigate the Type II SPDC in a potassium niobate ($KNbO_3$, KN) crystal, which is useful as a material platform for generating photon pairs of high spectral purity in the 2-μm spectral range. The technique is based on the frequency degenerate SPDC under Type II EPM for the high spectral purity of the biphoton states. First, we investigate the Type II EPM characteristics of KN in terms of the beam propagation direction, the spectral position of photon pairs, and the corresponding effective nonlinearities and beam walk-offs. We will then show that Type II EPM is feasible for a 1064-nm pumped SPDC under a moderate temperature condition, which is followed by the comparison of the effective nonlinear optic coefficients (d_{eff}) calculated under the given condition with those of other crystals using the Type II EPM. The result showed that the d_{eff} values of KN is 4.67, 4.03, and 7.44-times larger than those of PPKTP, PPLN, and $β$-BaB_2O_4 (BBO), respectively. The joint spectral analysis showed that a pair of photons with a wavelength of 2128 nm can be generated by a 1064-nm pumped Type II SPDC, with a high purity of 0.995 through proper pump filtering.

2. Materials and Theories

KN is a negative biaxial crystal belonging to the point group of orthorhombic mm^2 at room temperature, and its lattice constants are a = 0.56896 nm, b = 0.39692 nm, and c = 0.57256 nm [14,15]. The crystallographic axes (a, b, c) of KN are all perpendicular to each other and have a relationship of (a, b, c) = (y, x, z) with the optical axes. In this case, the order of refractive-index (RI) magnitudes is given by $n_z < n_y < n_x$. The temperature-dependent Sellmeier equations of KN are found in [16]. Figure 1a illustrates Type II SPDC in a KN, where an input pump photon with a frequency $2ω$ generates a pair of photons (signal and idler) with the same frequency $ω$ and polarization states perpendicular to each other. The collinear birefringent PM (BPM) is achieved between the wave vectors (**k**) of the pump, signal, and idler photons as shown in Figure 1b. However, their beam directions (i.e., Poynting vectors, **s**) are generally not parallel to the crystallographic axes of KN, resulting in a spatial walk-off due to the birefringence as shown in Figure 1c. This spatial walk-off will be discussed further in a later paragraph. The type II BPM condition can be expressed as:

$$\Delta k = \left| k^{(l)}(2ω) - k^{(h)}(ω) - k^{(l)}(ω) \right| = 0, \tag{1}$$

where each k represents the wave number of the interacting wave, and is defined as $k^{(m)}(jω) = (jω/c)n^{(m)}$. The unit k-vector is defined in a spherical coordinate as ($\sinθ\cosφ$, $\sinθφ$, $\cosθ$). Here, $θ$ and $φ$ are the polar and azimuthal angles, respectively. The RIs of the

two eigen-polarization modes of light traveling inside a KN are expressed as follows by solving the Fresnel equation of the wave normal [17]:

$$n^{(m)}(j\omega) = \sqrt{\frac{2}{-B_j \pm \sqrt{B_j^2 - 4C_j}}}. \tag{2}$$
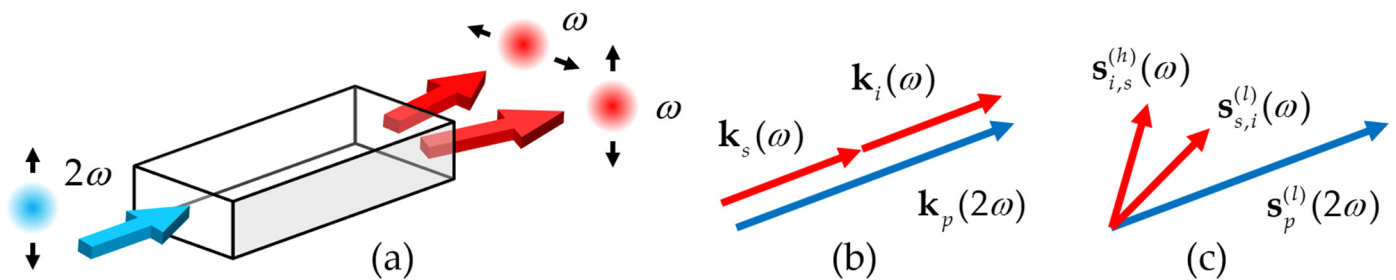
Figure 1. Schematic diagrams showing: (**a**) the relationships of frequencies and polarizations of pump, signal, and idler photons interacting via Type II spontaneous parametric down conversion (SPDC) in potassium niobate (KN), (**b**) the birefringent phase matching (BPM) between the wave vectors (**k**) of interacting waves, and (**c**) the spatial walk-off between the interacting beam lines described in the directions of Poynting vectors (**s**).

The parameters in Equation (2) are defined as follows:

$$B_j = -(b_j + c_j)k_x^2 - (a_j + c_j)k_y^2 - (b_j + a_j)k_z^2, \tag{3}$$

$$C_j = b_j c_j k_x^2 + a_j c_j k_y^2 + b_j a_j k_z^2, \tag{4}$$

$$a_j = n_x(j\omega), \ b_j = n_y(j\omega), \ c_j = n_z(j\omega), \tag{5}$$

where, each k_i represents the x, y, and z-axis components of the wave vector. j can be 1 or 2, then $n^{(m)}(2\omega)$ and $n^{(m)}(\omega)$ denote the RIs of the pump wave and the signal (or idler) wave with frequencies 2ω and ω, respectively. m in Equation (2) can be either l or h, representing low or high RI. l and h are obtained by taking plus and minus from the $\pm$ sign of the denominator in Equation (2), respectively. The temporal walk-off between the interacting photons due to the difference in GV can be defined as the time delay (ΔT) per unit crystal length as follows:

$$\frac{\Delta T}{L} \equiv \frac{\Delta n_g}{c}, \tag{6}$$

where L and Δn_g represent the crystal length and the group index difference between the interacting photons, respectively [18]. The GV matching for the Type II interaction is achieved when $\Delta n_g = 0$ in Equation (6), which can be simplified as:

$$2n_g^{(l)}(2\omega) = n_g^{(h)}(\omega) + n_g^{(l)}(\omega). \tag{7}$$

Each subscript g in Equation (7) represents the group index. Now, the Type II EPM shown in Figure 1a is defined as Equations (1) and (7) being satisfied simultaneously. Each of these equations is a function of three variables: the pump wavelength (λ_p), θ, and ϕ. Therefore, by solving a system of Equations (1) and (7) while changing λ_p, we can obtain the solution set of θ and ϕ, i.e., the direction of pump wave vector for the Type II EPM at the given λ_p. Thus, by sweeping the pump wave vector along the direction characterized by the solution set of θ and ϕ, we can continuously tune the resonant λ_p. This means that the spectral position of a photon pair can be selectively determined or tuned within the range of the solution sets while maintaining the high spectral purity of biphoton states. In contrast, for PPKN, Type II EPM can only be achieved at a single wavelength [18].

The effective nonlinear optic coefficients (d_{eff}) for a given direction of pump wave can generally be expressed as a linear combination of *d*-values as follows:

$$d_{eff} = \xi_1 d_{15} + \xi_2 d_{24} + \xi_3 d_{31} + \xi_4 d_{32} + \xi_5 d_{33}, \tag{8}$$

where the five *d*-values of KN are $d_{15} = 12.4 \pm 0.2$ pm/V, $d_{31} = 11.9 \pm 0.2$ pm/V, $d_{24} = 12.8 \pm 0.2$ pm/V, $d_{32} = 13.7 \pm 0.2$ pm/V, and $d_{33} = 20.6 \pm 0.2$ pm/V at 1064 nm [19,20]. Here, the coefficients ξ_i are determined by the relationship between the crystallographic axes and the optical axes in a biaxial crystal with the point symmetry mm^2 [21]. For a KN with the relationships of (y, x, z) = (a, b, c), the ξ-coefficients are given as follows:

$$\begin{aligned}
\xi_1 &= -AE(BCE - GH)(BCH + GE)) - AH(BCE - GH)^2, \\
\xi_2 &= -AE(BGH - CE)(BGE + CH) - AH(BGE + CH)^2, \\
\xi_3 &= -AE(BCE - GH)(BCH + GE), \\
\xi_4 &= -AE(BGH - CE)(BGE + CH), \\
\xi_5 &= -A^3 E^2 H,
\end{aligned} \tag{9}$$

where the angle-dependent parameters of *A*, *B*, *C*, *G*, *E*, and *H* correspond to $\sin\theta$, $\cos\theta$, $\sin\phi$, $\cos\phi$, $\sin\delta$, and $\cos\delta$, respectively. The angle δ introduced for convenience only is defined as:

$$\tan\delta \equiv \frac{2BGC}{A^2 \cot^2 V_z - B^2 G^2 + C^2}, \tag{10}$$

where V_z represents the angle between the *z*-axis and the optic axis of biaxial birefringence. For biaxial crystals with a relationship $n_z < n_y < n_x$, such as KN, V_z is given by:

$$\cos V_z = \frac{n_x (n_y^2 - n_z^2)^{1/2}}{n_y (n_x^2 - n_z^2)^{1/2}}. \tag{11}$$

Due to the RI dependence of V_z, d_{eff} is given as a function of three variables λ_p, θ, and ϕ. Thus, d_{eff} can be obtained by substituting the solution sets of λ_p, θ, and ϕ that satisfy the Type II EPM (i.e., Equations (1) and (7)). The SPDC efficiency is proportional to the square of d_{eff} for a given direction of beam propagation [13].

When a light beam travels inside a biaxial crystal with the point symmetry mm^2, the spatial walk-off between the wave vector and the Poynting vector occurs within the crystal, as depicted in Figure 1b,c [22]. The walk-off angle (ρ) can be expressed as:

$$\tan\rho_j^{(m)} \equiv \left\{ n^{(m)}(j\omega) \right\}^2 \left[\left(\frac{k_x}{\left\{ n^{(m)}(j\omega) \right\}^{-2} - a_j} \right)^2 + \left(\frac{k_y}{\left\{ n^{(m)}(j\omega) \right\}^{-2} - b_j} \right)^2 + \left(\frac{k_z}{\left\{ n^{(m)}(j\omega) \right\}^{-2} - c_j} \right)^2 \right]^{-1/2}, \tag{12}$$

where, all parameters of Equation (12) are defined in Equations (2)–(5). For the Type II EPM in biaxial crystals such as a KN, the relationships of Poynting vectors (**s**) of the interacting waves are illustrated in Figure 1c, while the BPM is collinear as shown in Figure 1b. The low-RI signal (or idler) beam ($\mathbf{s}_{s,i}^{(l)}$) is always placed between the high-RI idler (or signal) beam ($\mathbf{s}_{i,s}^{(h)}$) and the low-RI pump beam ($\mathbf{s}_p^{(l)}$) as shown in Figure 1c. In this case, the spatial walk-off between the interacting beams can be defined as the largest angle (*w*) formed by the Poynting vectors of the high-RI idler (or signal) beam and the low-RI pump beam:

$$\cos w = \cos\rho_1^{(h)} \cos\rho_2^{(l)}. \tag{13}$$

Here, *w* is also given as a function of three variables λ_p, θ, and ϕ, which can be obtained by substituting the solution sets of λ_p, θ, and ϕ satisfying the Type II EPM into Equation (13).

The maximum deviation between the interacting beams after passing through the crystal of length L is expressed as:

$$\Delta = L \tan w. \tag{14}$$

The joint spectral analysis is commonly used to quantify the heralded-state spectral purity of the SPDC output, which includes the construction of the signal-idler joint spectral amplitude (JSA) and the calculation of the purity of biphoton state via Schmidt decomposition [23–25]. Here, the spectral purity is a parameter that describes the degree of spectral uncorrelation between the signal and the idler photons. The signal-idler biphoton state $|\psi\rangle$ produced via SPDC can be expressed as:

$$|\psi\rangle = \int_0^\infty \int_0^\infty d\omega_s d\omega_i f(\omega_s, \omega_i) \hat{a}_s^\dagger(\omega_s) \hat{a}_i^\dagger(\omega_i) |0\rangle |0\rangle, \tag{15}$$

where $\hat{a}_s^\dagger$ and $\hat{a}_i^\dagger$ are the creation operators of the signal and idler photons, respectively, and ω_s and ω_i are the corresponding frequencies. The correlation function, $f(\omega_s, \omega_i)$, represents the biphoton JSA, and is defined as the product of pump envelop (PE) function and the PM function as follows:

$$f(\omega_s, \omega_i) \equiv N\alpha(\omega_s, \omega_i)\varphi(\omega_s, \omega_i). \tag{16}$$

Here, N denotes the normalization constant. If a pump with Gaussian spectral shape is assumed, the PE function can be written as:

$$\alpha(\omega_s, \omega_i) \propto \exp\left[-\frac{(\omega_s + \omega_i - \omega_p)^2}{\sigma_p^2}\right], \tag{17}$$

where ω_p and σ_p represent the center frequency and bandwidth of the pump, respectively. The PM function is given in the form of a sinc function as shown below:

$$\varphi(\omega_s, \omega_i) \propto \operatorname{sinc}\left(\frac{\Delta k L}{2}\right), \tag{18}$$

where Δk represents the phase-mismatch defined in Equation (1). For the given direction of the pump wave that satisfies the Type II EPM (i.e., the solution sets of θ and ϕ), Equation (18) is given as a function of the signal and idler wavelengths (or λ_s and λ_i), so the JSA can be plotted on a two-dimensional plane as a function of λ_s and λ_i. Then, the purity can be calculated via the following Schmidt decomposition:

$$f(\omega_s, \omega_i) = \sum_j \sqrt{c_j} |\zeta_{s,j}\rangle |\zeta_{i,j}\rangle, \tag{19}$$

where Schmidt coefficients, c_j, are a set of non-negative real numbers satisfying the normalization condition, $\sum_j c_j = 1$. $|\zeta_{s,j}\rangle$ and $|\zeta_{i,j}\rangle$ represent the orthonormal basis states called as Schmidt modes. Then the spectral purity, P, is defined as the sum of squares of Schmidt coefficients as [23–25]:

$$P = \sum_j c_j^2. \tag{20}$$

Therefore, once we plot the JSA as functions of λ_s and λ_i in a two-dimensional plane, P can be calculated via the Schmidt decomposition in Equation (20).

3. Simulations and Discussion

Figure 2a shows the BPM and GV matching properties of SPDC in a KN at 22 °C. The blue and the cyan surfaces represent the BPM and GV surfaces calculated using Equations (1) and (7), respectively. The vertical axis represents the wavelength of the pump photon (λ_p), and the base of the coordinates is the plane formed by the angles θ and ϕ indicating the direction of the pump wave vector. The intersection line of the two surfaces

in Figure 2a spans a specific range characterized by λ_p, θ, and ϕ, which corresponds to the Type II EPM. This is more clearly plotted in Figure 2b. Here, the blue line represents the intersection of the two surfaces, and the green and red lines represent the projections of the blue line on the ϕ-λ_p and θ-λ_p planes, respectively. The range of λ_p resonance that satisfies the Type II EPM is 1044.95–1062.78 nm at 22 °C, which corresponds to the ϕ-range 90–0° and the θ-range 41.0–63.8° as plotted in Figure 2b. It shows that the Type II EPM is achievable for all azimuthal angles, whereas for polar angles only in a specific angular region. The type II EPM properties of KN are summarized in Table 1.
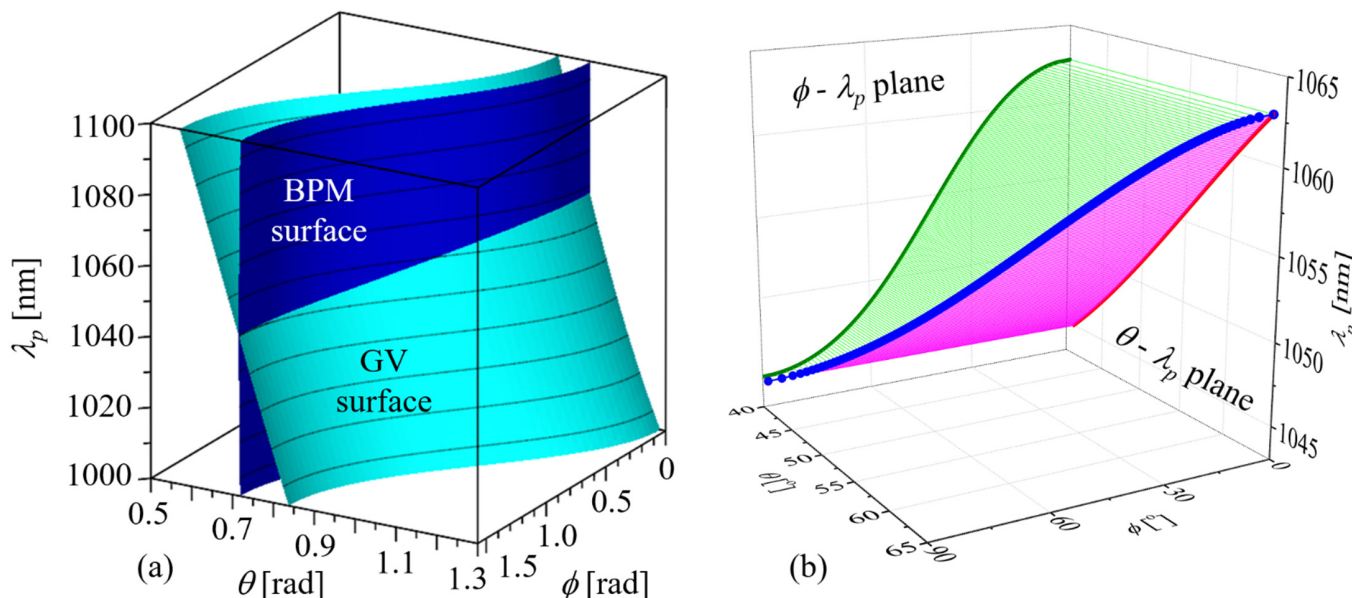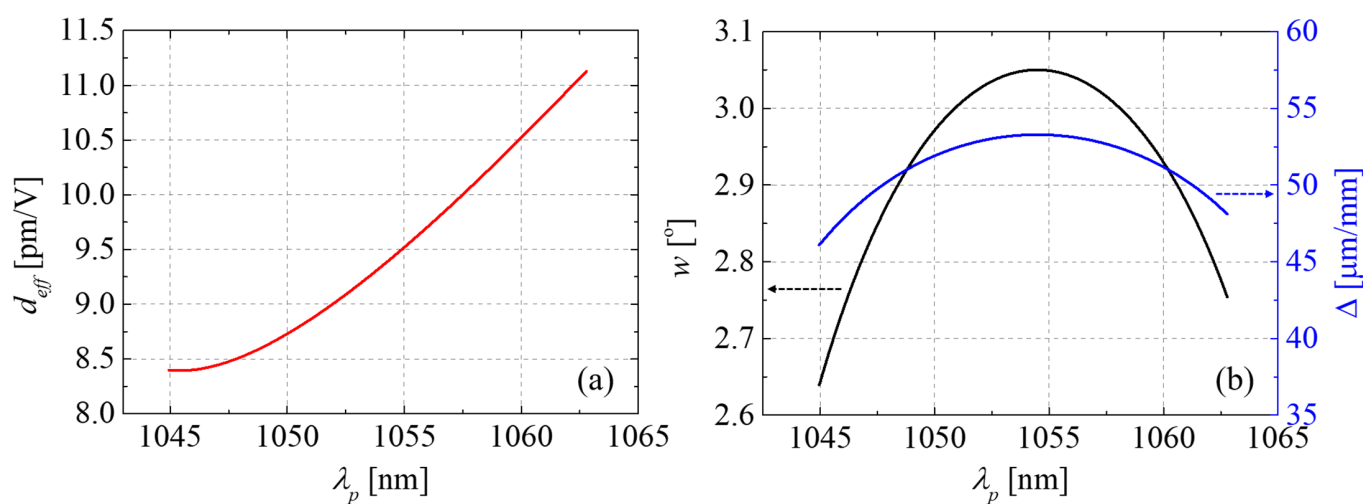

Figure 2. (**a**) Numerical simulation results of the BPM and the group velocity (GV) matching for SPDC in a KN at 22 °C; (**b**) Type II extended phase matching (EPM) property of KN (the blue line) and its projections on the ϕ-λ_p and θ-λ_p planes (the green and red lines, respectively).

Table 1. The type II EPM properties of KN at 22 °C: the resonant pump wavelength (λ_p) and the corresponding signal/idler wavelengths (λ_s and λ_i), the BPM direction (θ, ϕ), the effective nonlinear optic coefficient (d_{eff}), the spatial walk-off angle (w) between the interacting beams, and the beam deviation (Δ).

Physical Quantities	Range of Values
λ_p (nm)	1044.95–1062.78
λ_s (or λ_i) (nm)	2089.90–2125.55
ϕ (°)	90–0
θ (°)	41.00–63.80
d_{eff} (pm/V)	8.40–11.13
w (°)	2.64–3.05
Δ (µm/mm)	46.10–53.29

The magnitude of the effective nonlinear optic coefficient (d_{eff}) is determined by the BPM direction as described in the paragraphs with Equations (8)–(11). Since the efficiency of SPDC is proportional to the square of d_{eff}, it is important to estimate the d_{eff}-values for the given direction of wave vectors satisfying the Type II EPM. The d_{eff}-values were calculated numerically using Equations (8)–(11), and the results are plotted in Figure 3a as a function of λ_p. The horizontal width of the graph falls within the full range of λ_p that satisfies the Type II EPM. In this range, the d_{eff} values span 8.40–11.13 pm/V, which are much larger than other cases using the Type II EPM approach, e.g., d_{eff} = 1.50 pm/V for BBO under the BPM; 2.39 pm/V (=$(2/\pi)d_{24}$) for PPKTP and 2.77 pm/V (=$(2/\pi)d_{15}$) for PPLN, under the

first-order QPM [10,26,27]. The largest values of d_{eff} are 11.13 pm/V at 1062.78 nm, and the corresponding BPM direction is $(\theta, \phi) = (63.8°, 0°)$. It is noteworthy that the d_{eff}-value is the largest when the wave vectors for the BPM are parallel to the *x-z* plane ($\phi = 0$). The maximum walk-off angle (w) between the interacting beams and the corresponding beam deviation (Δ) were calculated using Equations (13) and (14), respectively, and plotted together in Figure 3b as a function of λ_p that satisfies the Type II EPM. Over the whole range of λ_p, the calculated w value spans 2.64–3.05°. The deviation (Δ) between the interacting beams per crystal of unit millimeter length is 46.10–53.29 µm/mm, which can be sufficiently overcome by using a pump beam of large size in thick crystals. The calculated values of d_{eff}, w, and Δ are also summarized in Table 1.

Figure 3. (**a**) The effective nonlinear optic coefficient (d_{eff}); (**b**) the spatial walk-off angle (w) between the interacting beams, and the beam deviation (Δ). The numerical simulation results were plotted as functions of λ_p satisfying the Type II EPM.

Now, for the case with the largest d_{eff} value (i.e., $\phi = 0$), the temperature behaviors of Type II EPM characteristics of KN are investigated. Figure 4a shows the change in λ_p resonance and the corresponding polar angle (θ), as a function of temperature, *t*. As the temperature rises from 20 to 130 °C, λ_p shifts to longer wavelengths (1062.68 nm → 1070.06 nm), while the polar angle for Type II EPM only increases by 2.6° from 68.8°. Since the azimuthal angle is always $\phi = 0$ for the case with the largest d_{eff} value, only the polar angle needs to be fine-tuned to maintain Type II EPM while the temperature rises. At $t = 45.59$ °C, the λ_p resonance reaches 1064 nm, which is the center wavelength of typical Nd:YAG lasers. This means that, without preparing a light source suitable for the resonance of the crystal for SPDC, high-purity photon pairs can be generated under moderate temperature conditions using a commercial high-power laser. High power SPDC pumping within the laser damage threshold of the crystal, along with the largest nonlinearity, can increase the maximum number of photon pairs per second. While the temperature rises from 20 to 130 °C, the d_{eff} value increases slightly from 11.12 to 11.36 pm/V, as shown in Figure 4b. The d_{eff} value of KN calculated at $t = 45.59$ °C (or $\lambda_p = 1064$ nm) is 11.16 pm/V, which is 4.67, 4.03, and 7.44-times larger than those of PPKTP, PPLN, and BBO using the Type II EPM approach, respectively. These values correspond to 21.80, 16.24, and 55.40-times increases in SPDC efficiency, respectively, because the nonlinear optic efficiency is proportional to the square of d_{eff} [13]. Here, we note that the generation of photon pairs based on the Type II SPDC in the 2-µm band is also feasible in KTP isomorphs, but, in this case, 1064-nm pumping is not possible and the effective nonlinearity is much smaller than that of KN [28]. To the best of our knowledge, the generation of photon pairs based on the Type II EPM SPDC in biaxial birefringent crystals with orthorhombic mm^2 point symmetry (e.g., KN and non-poled KTP isomorphs) has not yet been experimentally demonstrated, nor has the 1064-nm

pumped case. We highlight that the generation of photon pairs is possible with high efficiency and high spectral purity based on 1064-nm pumped Type II SPDC in KN. We believe that KN can be the best candidate for this purpose. Experimental demonstrations are currently underway using commercially available bulk KN crystals [29]. The crystal most similar to KN in its constituent atoms is lithium niobate (LiNbO$_3$ or LN). LN is "nonlinear optically" different from KN in that it belongs to the trigonal 3 m point group and exhibits uniaxial birefringence. Several studies on the photon-pair generation using PPLNs have been reported so far, but in all of the cases the EPM approach was not used or the frequencies of the generated photon pairs were not degenerated [30–34]. Experimental results for the generation of photon pairs in thin-film PPLN have only been reported recently, but again, Type 0 SPDC were used [35,36]. The frequency-degenerate, Type II EPM approach for LN has recently been reported only as a theoretical study [26]. However, for non-poled LNs, the effective nonlinearity (and thus the SPDC efficiency) is too low as $d_{eff} \leq 0.2$ pm/V, and for PPLNs, the wavelength of the photon pair is longer than 3.5 μm (with $d_{eff} \sim 4$ pm/V), which is far from the 2-μm band (or 1064-nm pumping). For a 1064-nm-pumped SPDC in KN, the spectral position of a photon pair is 2128 nm, which is within the high transparency range in the atmospheric absorption spectrum [5]. The spatial walk-off angle (w) between the interacting photons and the corresponding beam deviation (Δ) calculated using Equations (13) and (14), respectively, are 3.20° and 55.89 μm/mm, respectively. Since these values are smaller than those of BBO (i.e., $w = 3.5°$ and $\Delta = 61.16$ μm/mm), which are widely used for the photon-pair generation, longer nonlinear interaction lengths within the crystals can be used to increase SPDC efficiency. For the case with the maximum d_{eff} value, the Type II EPM conditions at $\lambda_p = 1064$ nm are listed in Table 2.
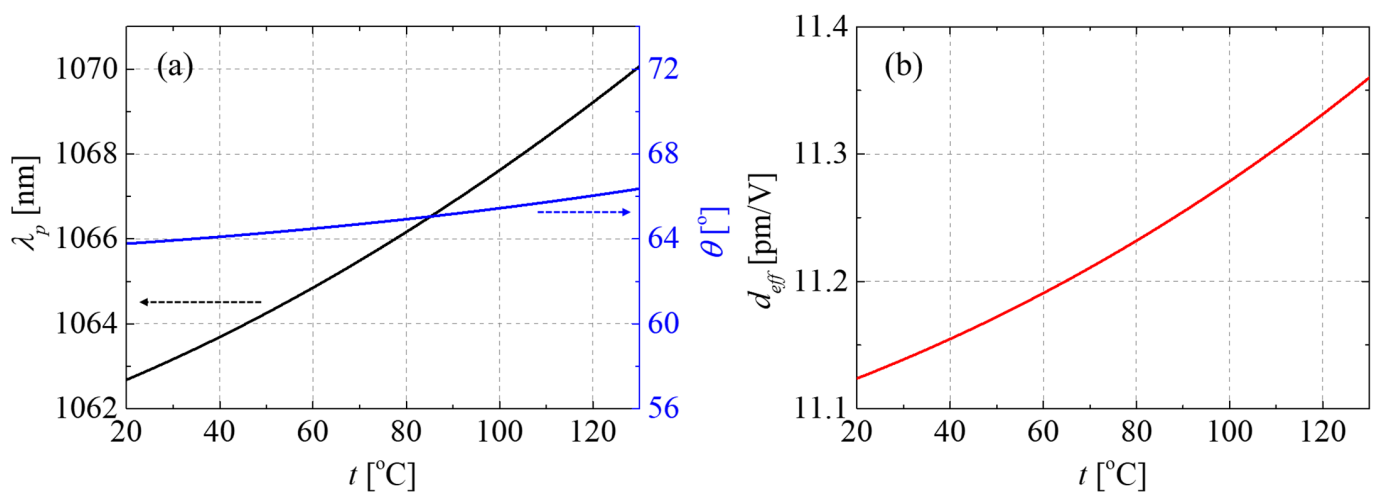
Figure 4. For the case with the largest d_{eff} value (i.e., $\phi = 0$) under Type II EPM, the temperature dependence of: (**a**) the λ_p resonance and the corresponding polar angle (θ) and (**b**) the d_{eff} values plotted as a function of t.

To quantify the heralded-state spectral purity of the SPDC output, we now analyze the signal-idler JSA properties, including the calculation of the purity of the biphoton state. Figure 5 shows the JSA characteristics of Type II SPDC for the case of KN listed in Table 2 (i.e., $\lambda_p = 1064$ nm, the maximum d_{eff}, Type II EPM). Figure 5a,b shows density plots of the PE and PM functions calculated using Equations (17) and (18), respectively, for a pump with a linewidth of 2.43 nm. This level of linewidth can be easily achieved through a combination of several filters placed in series because bandpass filters for pump filtering in the 1-μm band are commercially available with a high technical level. The joint spectral intensity (JSI) calculated using Equation (16) is shown in Figure 5c, where JSI is defined as |JSA|^2. Here, the crystal length of 10 mm is used for all calculations. All of the density plots in Figure 5a–c are displayed in a 40 nm × 40 nm window. The solid (blue) and dashed (red) lines in Figure 5d represent the contour lines for JSI = 0.5 and a circle with a diameter

of 8.1 nm, respectively. The contour line represents a circular shape, and the spectral purity calculated using Schmidt decomposition in Equation (20) reaches 0.995. The results show that at a wavelength of 2128 nm, very high spectral purity photon pairs can be generated in KN via a 1064-nm pumped SPDC with a Type II EPM approach.

Table 2. For the case with the maximum d_{eff} value, the Type II EPM conditions where the resonance of the pump photon is located at the center wavelength of Nd:YAG lasers (i.e., 1064 nm).

Physical Quantities	Values
t (°C)	45.59
λ_p (nm)	1064.00
λ_s (or λ_i) (nm)	2128.00
ϕ (°)	0
θ (°)	45.59
d_{eff} (pm/V) [1]	11.16
w (°)	3.20
Δ (μm/mm)	55.89

[1] cf. d_{eff} = 1.50 pm/V for BBO under the BPM; 2.39 pm/V (=$(2/\pi)d_{24}$) for PPKTP and 2.77 pm/V (=$(2/\pi)d_{15}$) for PPLN, under the first-order QPM.
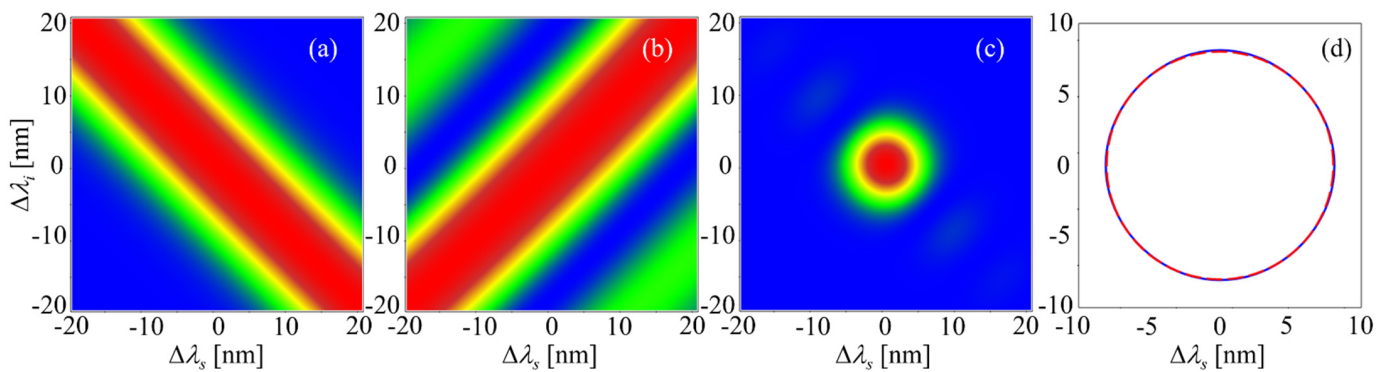
Figure 5. JSA characteristics of the SPDC output for the case of KN listed in Table 2 (i.e., λ_p = 1064 nm, the maximum d_{eff}, Type II EPM): (**a**) the pump envelope (PE) function, (**b**) the phase matching (PM) function, (**c**) the joint spectral intensity (JSI), and (**d**) the contour line for JSI = 0.5 (blue solid line) shown with a circle with a diameter of 8.1 nm (red dashed line). The spectral purity calculated using Schmidt decomposition is 0.995.

4. Conclusions

We have theoretically and numerically investigated the Type II SPDC properties of KN. We theoretically described the Type II EPM characteristics of KN, in terms of BPM, GV matchings, effective nonlinearities, and spatial walk-offs between the interacting photons. The numerical simulation results showed that the spectral position of photon pairs can be tuned within the range of 2089.90–2125.55 nm by sweeping the pump wave vector along the direction satisfying the Type II EPM condition at 22 °C. As the temperature of the KN rises from 20 to 130 °C, the pump wavelength that satisfies the Type II EPM shifts from 1062.68 to 1070.06 nm. The maximum effective nonlinearity (or SPDC efficiency) could be achieved when the wave vectors for the BPM are parallel to the *x–z* plane. For the case with the largest d_{eff}, the Type II EPM is practically feasible for a 1064-nm pumped SPDC at t = 45.59 °C. In this case, the spectral position of a photon pair is 2128 nm, which is within the high transparency range in the atmospheric absorption spectrum. The photon-pair source in this band has great potential for applications such as free space quantum communication and sensing, with the advantages of high sensitivity and low noise measurement. The d_{eff} value of KN is 4.67, 4.03, and 7.44-times larger than those of PPKTP, PPLN, and BBO, respectively, which means a significant improvement in SPDC efficiency. The heralded-state spectral purity of SPDC output was quantified via JSA analysis, and the results show that the purity calculated for a pump with a 2.43-nm bandwidth is as high as 0.995.

References

1. Mansell, G.L.; McRae, T.G.; Altin, P.A.; Yap, M.J.; Ward, R.L.; Slagmolen, B.J.J.; Shaddock, D.A.; McClelland, D.E. Observation of squeezed light in the 2 μm region. *Phys. Rev. Lett.* **2018**, *120*, 203603. [CrossRef]
2. Shields, T.; Prabhakar, S.; Powell, D.; Taylor, G.G.; Morozov, D.; Ebrahim, M.; Kues, M.; Caspani, L.; Gawith, C.; Hadfield, R.H.; et al. Photon pair generation at 2080 μm by down-conversion. In Proceedings of the 2019 Conference on Lasers and Electro-Optics Europe & European Quantum Electronics Conference (CLEO/Europe-EQEC), Munich, Germany, 23–27 June 2019.
3. Prabhakar, S.; Shields, T.; Dada, A.C.; Ebrahim, M.; Taylor, G.G.; Morozov, D.; Erotokritou, K.; Miki, S.; Yabuno, M.; Terai, H.; et al. Two-photon quantum interference and entanglement at 2.1 μm. *Sci. Adv.* **2020**, *6*, eaay5195. [CrossRef]
4. Steinlechner, J.; Martin, I.W.; Bell, A.S.; Hough, J.; Fletcher, M.; Murray, P.G.; Robie, R.; Rowan, S.; Schnabel, R. Silicon-based optical mirror coatings for ultrahigh precision metrology and sensing. *Phys. Rev. Lett.* **2018**, *120*, 263602. [CrossRef]
5. Gemini Observatory. Available online: https://www.gemini.edu/observing/telescopes-and-sites/sites#Transmission (accessed on 16 April 2021).
6. Kaushal, H.; Kaddoum, G. Optical communication in space: Challenges and mitigation techniques. *IEEE Commun. Surv. Tutor.* **2017**, *19*, 57–96. [CrossRef]
7. Giovannetti, V.; Maccone, L.; Shapiro, J.H.; Wong, F.N.C. Extended phase-matching conditions for improved entanglement generation. *Phys. Rev. A* **2002**, *66*, 043813. [CrossRef]
8. Kuzucu, O.; Fiorentino, M.; Albota, M.A.; Wong, F.N.C.; Kärtner, F.X. Two-photon coincident-frequency entanglement via extended phase matching. *Phys. Rev. Lett.* **2005**, *94*, 083601. [CrossRef] [PubMed]
9. Kwiat, P.; Mattle, K.; Weinfurter, H.; Zeilinger, A.; Sergienko, A.V.; Shih, Y. New high-intensity source of polarization-entangled photon pairs. *Phys. Rev. Lett.* **1995**, *75*, 4337–4341. [CrossRef]
10. Jin, R.-B.; Shimizu, R.; Wakui, K.; Fujiwara, M.; Yamashita, T.; Miki, S.; Terai, H.; Wang, Z.; Sasaki, M. Pulsed Sagnac polarization-entangled photon source with a PPKTP crystal at telecom wavelength. *Opt. Express* **2014**, *22*, 11498–11507. [CrossRef] [PubMed]
11. Weston, M.M.; Chrzanowski, H.M.; Wollmann, S.; Boston, A.; Ho, J.; Shalm, L.K.; Verma, V.B.; Allman, M.S.; Nam, S.W.; Patel, R.B.; et al. Efficient and pure femtosecond-pulse-length source of polarization-entangled photons. *Opt. Express* **2016**, *24*, 10869–10879. [CrossRef] [PubMed]
12. Koechner, W. *Solid-State Laser Engineering*, 6th ed.; Springer: New York, NY, USA, 2006; pp. 54–61.
13. Boyd, R.W. *Nonlinear Optics*, 4th ed.; Academic Press: San Diego, CA, USA, 2020; pp. 70–73.
14. Uematsu, Y. Nonlinear optical properties of $KNbO_3$ single crystals in the orthorhombic phase. *Jpn. J. Appl. Phys.* **1974**, *13*, 1362–1368. [CrossRef]
15. Zysset, B.; Biaggio, I.; Günter, P. Refractive indices of orthorhombic $KNbO_3$. I. Dispersion and temperature dependence. *J. Opt. Soc. Am. B* **1992**, *9*, 380–386. [CrossRef]
16. Jundt, D.H.; Gunter, P.; Zysset, B. A temperature-dependent dispersion equation for $KNbO_3$. *Nonlinear Opt.* **1993**, *4*, 341–345.
17. Yariv, A.; Yeh, P. *Photonics: Optical Electronics in Modern Communications*, 6th ed.; Oxford University Press: New York, NY, USA, 2007; pp. 30–33.
18. Lee, K.J.; Lee, S.; Shin, H. Extended phase matching properties of periodically poled potassium niobate crystals for mid-infrared polarization-entangled photon-pair generation. *Appl. Opt.* **2016**, *55*, 9791–9796. [CrossRef]
19. Baumert, J.-C.; Hoffnagle, J.; Günter, P. Nonlinear optical effects in $KNbO_3$ crystals at $Al_xGa_{1-x}As$, dye, ruby and Nd:YAG laser wavelengths. *Proc. SPIE* **1984**, *492*, 374–385.
20. Roberts, D.A. Simplified characterization of uniaxial and biaxial nonlinear optical crystals: A plea for standardization of nomenclature and conventions. *IEEE J. Quantum Electron.* **1992**, *28*, 2057–2074. [CrossRef]
21. Dmitriev, V.G.; Nikogosyan, D.N. Effective nonlinearity coefficients for three-wave interactions in biaxial crystals of mm^2 point group symmetry. *Opt. Commun.* **1993**, *95*, 173–182. [CrossRef]
22. Brehat, F.; Wyncke, B. Calculation of double-refraction walk-off angle along the phase-matching directions in nonlinear biaxial crystals. *J. Phys. B At. Mol. Opt. Phys.* **1989**, *22*, 1891–1898. [CrossRef]

23. Grice, W.P.; Walmsley, I.A. Spectral information and distinguishability in type-II down-conversion with a broadband pump. *Phys. Rev. A* **1997**, *56*, 1627. [CrossRef]

24. Law, C.K.; Walmsley, I.A.; Eberly, J.H. Continuous frequency entanglement: Effective finite Hilbert space and entropy control. *Phys. Rev. Lett.* **2000**, *84*, 5304. [CrossRef] [PubMed]

25. Mosley, P.J.; Lundeen, J.S.; Smith, B.J.; Walmsley, I.A. Conditional preparation of single photons using parametric downconversion: A recipe for purity. *New J. Phys.* **2008**, *10*, 093011. [CrossRef]

26. Kim, I.; Lee, D.; Lee, K.J. Study of Type II SPDC in lithium niobate for high spectral purity photon pair generation. *Crystals* **2021**, *11*, 406. [CrossRef]

27. Shoji, I.; Nakamura, H.; Ohdaira, K.; Kondo, T.; Ito, R.; Okamoto, T.; Tatsuki, K.; Kubota, S. Absolute measurement of second-order nonlinear-optical coefficients of β-BaB$_2$O$_4$ for visible to ultraviolet second-harmonic wavelengths. *J. Opt. Soc. Am. B* **1999**, *16*, 620–624. [CrossRef]

28. Kim, I.; Lee, D.; Lee, K.J. Numerical investigation of high-purity polarization-entangled photon-pair generation in non-poled KTP isomorphs. *Appl. Sci.* **2021**, *11*, 565. [CrossRef]

29. CRYLINK. Available online: https://www.laser-crylink.com/laser-products/nonlinear-crystal/knbo3 (accessed on 20 May 2021).

30. Fujii, G.; Namekata, N.; Motoya, M.; Kurimura, S.; Inoue, S. Bright narrowband source of photon pairs at optical telecommunication wavelengths using a type-II periodically poled lithium niobate waveguide. *Opt. Express* **2007**, *15*, 12769–12776. [CrossRef]

31. Martin, A.; Issautier, A.; Herrmann, H.; Sohler, W.; Ostrowsky, D.B.; Alibart, O.; Tanzilli, S. A polarization entangled photon-pair source based on a type-II PPLN waveguide emitting at a telecom wavelength. *New J. Phys.* **2010**, *12*, 103005. [CrossRef]

32. Cheng, X.; Sarihan, M.C.; Chang, K.-C.; Lee, Y.S.; Laudenbach, F.; Ye, H.; Yu, Z.; Wong, C.W. Design of spontaneous parametric down-conversion in integrated hybrid Si$_x$N$_y$-PPLN waveguides. *Opt. Express* **2019**, *27*, 30773–30787. [CrossRef]

33. Kuo, P.S.; Verma, V.B.; Nam, S.W. Demonstration of a polarization-entangled photon-pair source based on phase-modulated PPLN. *OSA Contin.* **2020**, *3*, 295–304. [CrossRef]

34. Kuo, P.S.; Gerrits, T.; Verma, V.; Nam, S.W.; Slattery, O.; Ma, L.; Tang, X. Characterization of type-II spontaneous parametric down-conversion in domain-engineered PPLN. *Proc. SPIE Adv. Photonics Quantum Comput. Mem. Commun.* **2016**, *9762*, 976211.

35. Zhao, J.; Ma, C.; Rüsing, M.; Mookherjea, S. High quality entangled photon pair generation in periodically poled thin-film lithium niobate waveguides. *Phys. Rev. Lett.* **2020**, *124*, 163603. [CrossRef]

36. Chen, J.-Y.; Sua, Y.M.; Ma, Z.-H.; Tang, C.; Li, Z.; Huang, Y.-P. Efficient parametric frequency conversion in lithium niobate nanophotonic chips. *OSA Contin.* **2019**, *2*, 2914–2924. [CrossRef]